Supporting Information

Investigating the formation of metal nitride complexes employing a tetradentate bis-carbene bis-phenolate ligand

Romain Kunert,[a,b] Diego Martelino,[a] Samyadeb Mahato,[a] Nick Hein,[a] Jason Pulfer,[a] Christian Philouze,[b] Oliver Jarjayes,[b*] Fabrice Thomas,[b*] Tim Storr[a*]

[a]Department of Chemistry, Simon Fraser University, Burnaby, British Columbia, V5A 1S6, Canada. Email: tim_storr@sfu.ca

[b]Univ. Grenoble Alpes, CNRS, DCM, F-38000, Grenoble, France. Email: Olivier.Jarjayes@univ-grenoble-alpes.fr; Fabrice.Thomas@univ-grenoble-alpes.fr

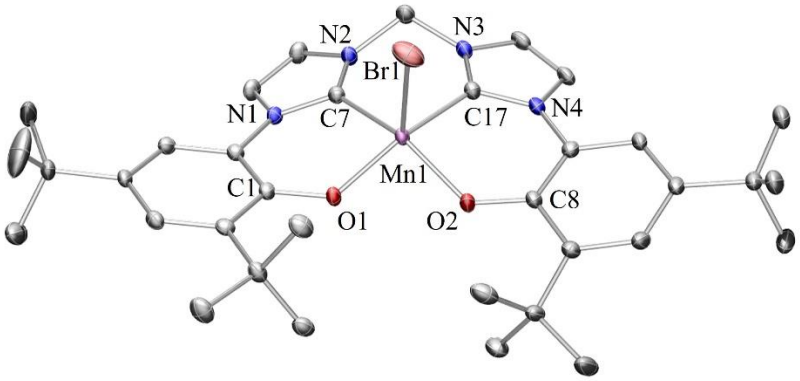

Figure S1. POV-ray representation of **MnL^{C2O2}Br**. Thermal ellipsoids shown at 50% probability level. Hydrogen atoms were omitted for clarity. Mn, pink; C, gray; O, red; N, blue. Select interatomic distances [Å] and angles [deg]: Mn(1)−O(1): 1.881(1), Mn(1)−O(2): 1.898(1), Mn(1)−C(7): 2.026(2), Mn(1)−C(17): 2.028(2), Mn(1)−Br(1): 2.5498(4).

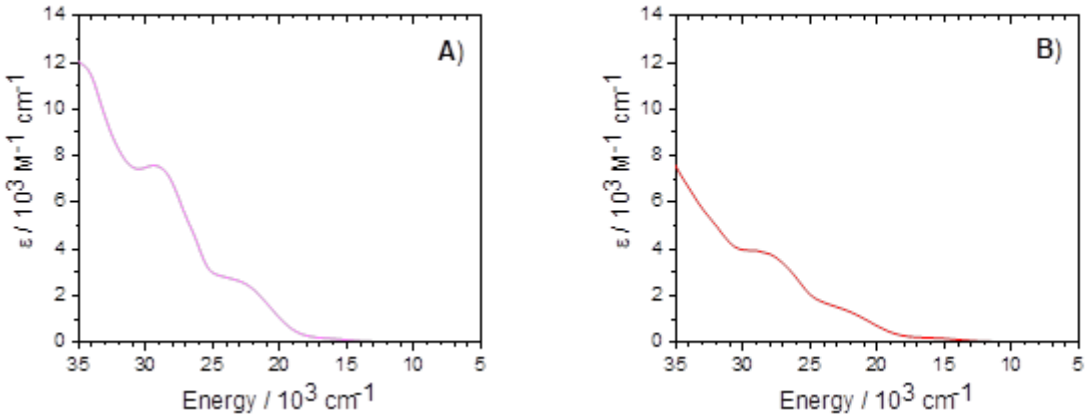

Figure S2. UV-vis-NIR spectra of **MnL^{C2O2}(Br)** (**A**) and **MnL^{C2O2}(N$_3$)** (**B**) in CH_2Cl_2; T = 298 K.

Table S1. Crystal data and structure refinement for **MnL^{C2O2}(Br)**, **MnL^{C2O2}(N$_3$)** and **[H$_2$L^{C2O2}(N)]Cl**.

Compound	**MnL^{C2O2}(Br)**	**MnL^{C2O2}(N$_3$)**	**[H$_2$L^{C2O2}(N)]Cl**
CCDC Number	2359452	2359453	2359456
Formula	$C_{35}H_{46}BrMnN_4O_2$	$C_{35}H_{46}MnN_{6.97}Br_{0.03}O_2$	Cl, $C_{35}H_{48}N_5O_2$, H_2O, (0.748)CH_2Cl_2, (1.25)C_2H_3N
F_w [g.mol^{-1}]	689.61	653.47	739.08
T [K]	296(2)	273(2)	210
Morphology	needle	blade	prism
Color	brown	red	yellow
Crystal size [mm]	1 x 0.1 x 1	0.04 x 0.07 x 0.37	0.11 x 0.21 x 0.22
Crystal system	monoclinic	monoclinic	triclinic
Space group	C 2/c	P 2/n	P-1
a [Å]	30.477(2)	15.6595(7)	8.1811(16)
b [Å]	15.0603(11)	9.0777(5)	13.290(3)
c [Å]	20.2126(14)	25.7615(13)	20.518(4)
α [°]	90	90	96.27(3)
β [°]	122.3273(18)	90.347(2)	96.47(3)
γ [°]	90	90	106.01(3)
Unit-cell volume [Å^3]	7839.5(10)	3662.0(3)	2107.6(8)
Z	8	4	2
Dx [g.cm^{-3}]	1.169	1.185	1.165
μ [mm^{-1}]	1.387	0.429	0.226
F(000)	2880.0	1387.0	790.0

Radiation	MoKα (λ = 0.71073 Å)	MoKα (λ = 0.71073 Å)	MoKα (λ = 0.71073 Å)
Θ range for data collection/°	1.581 to 28.737	1.526 to 22.533	2.392 to 24.997
Index ranges	-41 ≤ h ≤ 41 -20 ≤ k ≤ 20 -27 ≤ l ≤ 27	-16 ≤ h ≤ 16 -9 ≤ k ≤ 9 -27 ≤ l ≤ 27	-9 ≤ h ≤ 9 -15 ≤ k ≤ 15 -24 ≤ l ≤ 24
Total reflections	165068	29267	33145
Unique reflections	10145	4778	7349
Used reflections	7774 (I>2σ(I))	3777 (I>2σ(I))	5498 (I>2σ(I))
Refined parameters	400	459	588
Rint.	0.0721	0.0583	0.0719
R1	0.0382	0.0331	0.0642
R(w)[a]	0.0935	0.0768	0.1819
Goodness of fit *S*	1.042	1.018	1.088
$\Delta\rho_{min}/\Delta\rho_{max}$ (e·Å^{-3})	-1.55/1.4	-0.23/0.27	-0.35/0.47

[a]Based on F^2 where $w = 1/[\sigma^2(Fo^2)+(0.0389P)^2+14.4630P]$ where $P=(Fo^2+2Fc^2)/3$ for **MnL^{C2O2}Br**

$w = 1/[\sigma^2(Fo^2)+(0.1000P)^2]$ where $P=(Fo^2+2Fc^2)/3$ for **MnL^{C2O2}(N$_3$)**

$w = 1/[\sigma^2(Fo^2)+(0.0816P)^2+1.4607P]$ where $P=(Fo^2+2Fc^2)/3$ for **[H$_2$L^{C2O2}(N)]Cl**

$w = 1/[\sigma^2(Fo^2)+(0.1062P)^2+2.1078P]$ where $P=(Fo^2+2Fc^2)/3$ for **1**

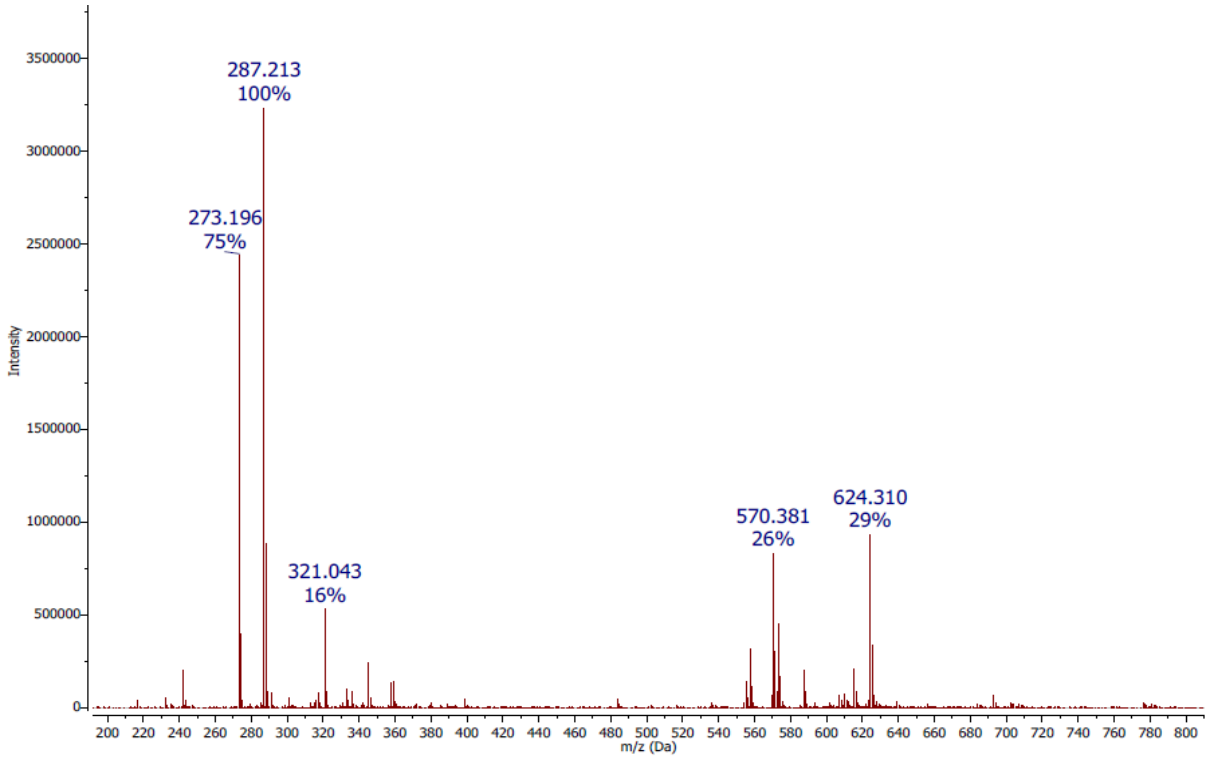

Figure S3. Positive mode ESI-MS analysis of the nitride exchange reaction between **Mnsalen(N)** and **MnL^{C2O2}(Br)** in CH_3CN.

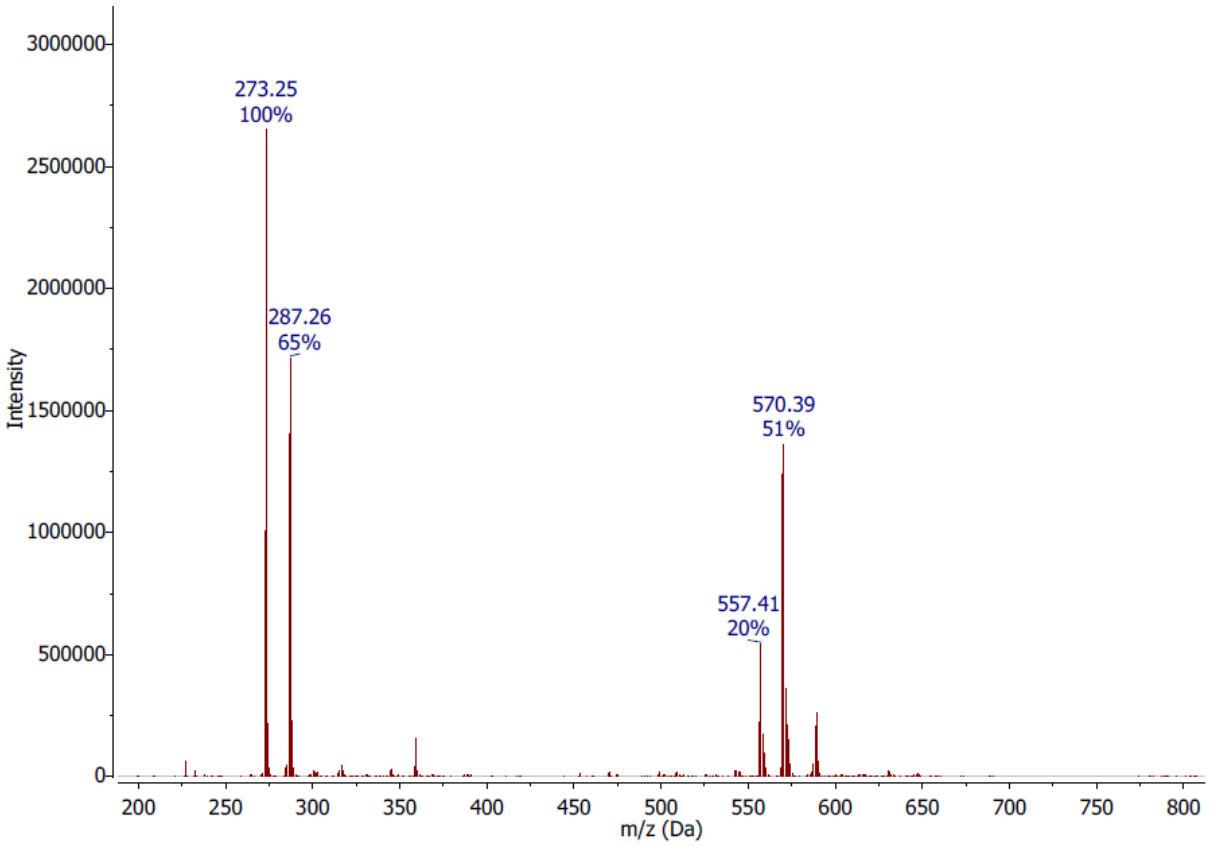

Figure S4. Positive mode ESI-MS analysis of a diethyl ether solution of the insertion reaction after washing with 10% HCl and EDTA.

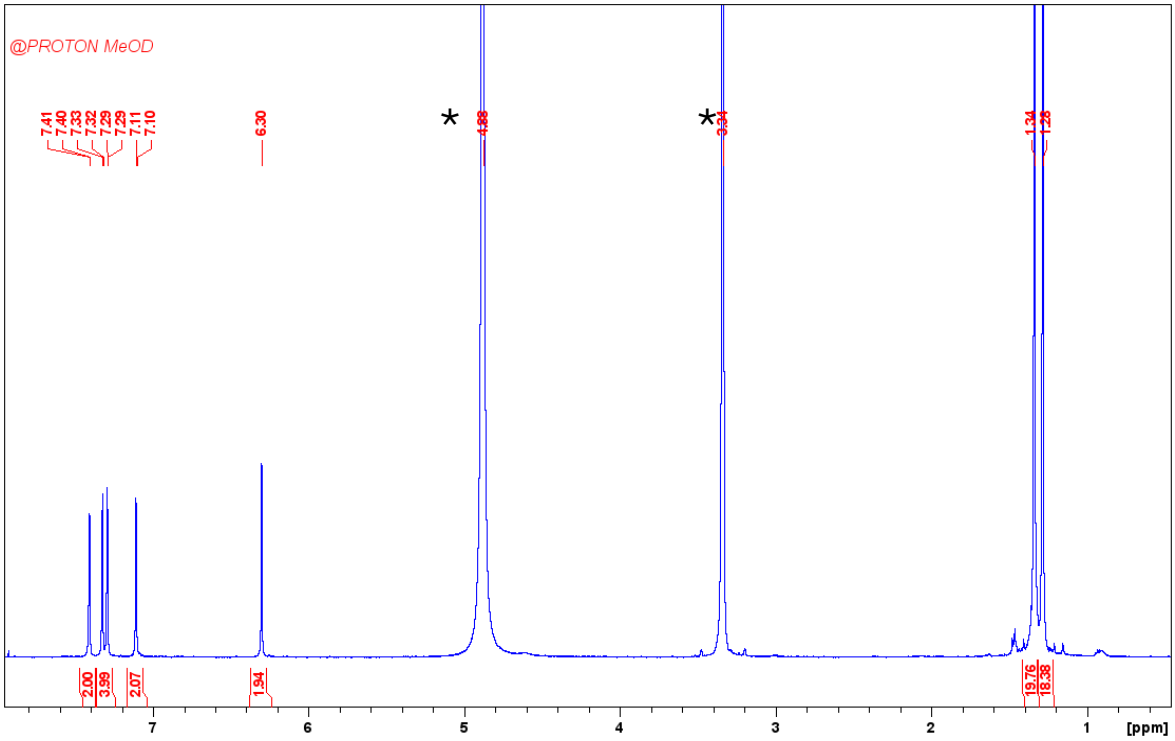

Figure S5. ^{1}H NMR spectrum of N-insertion product **[H_2L^{C2O2}(N)]Cl** in CD_3OD. Residual solvent from recrystallization marked with asterisks.

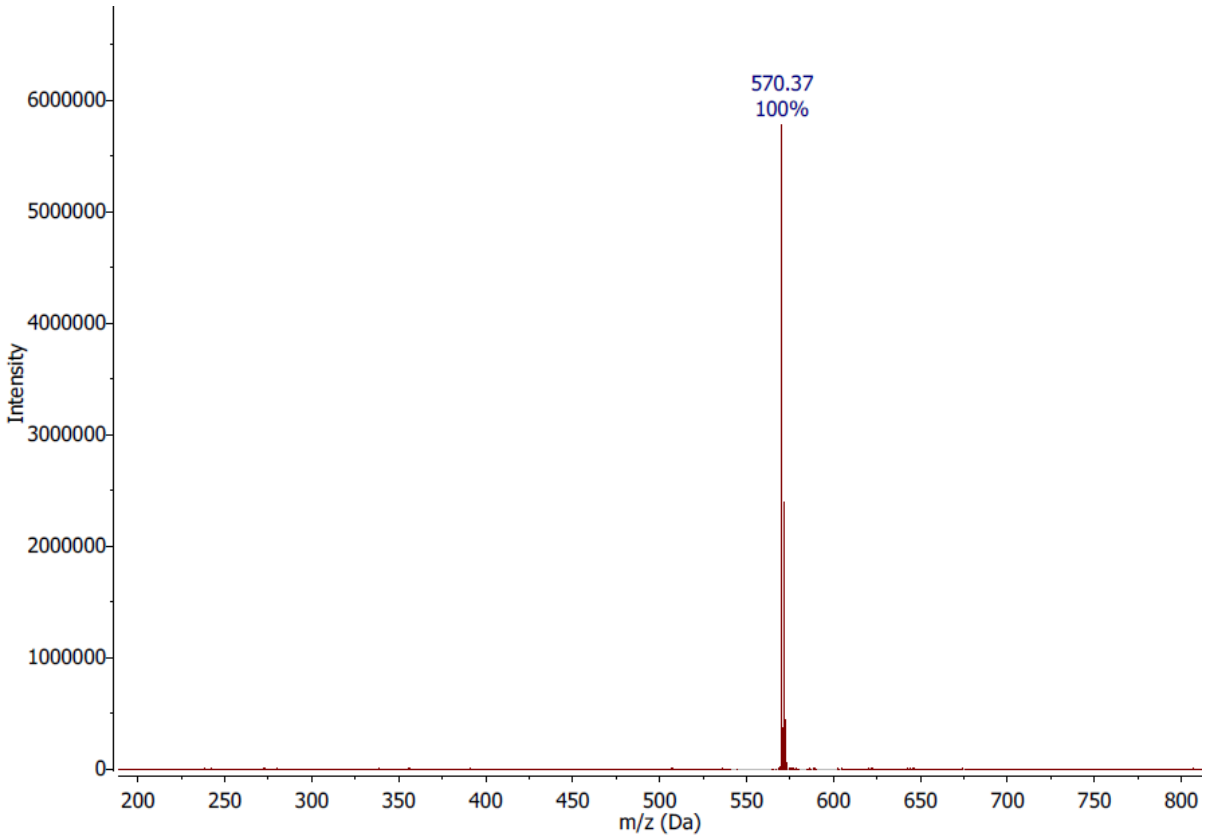

Figure S6. Positive mode ESI-MS of the N-insertion product **$[H_2L^{C2O2}(N)]Cl$** after recrystallization.

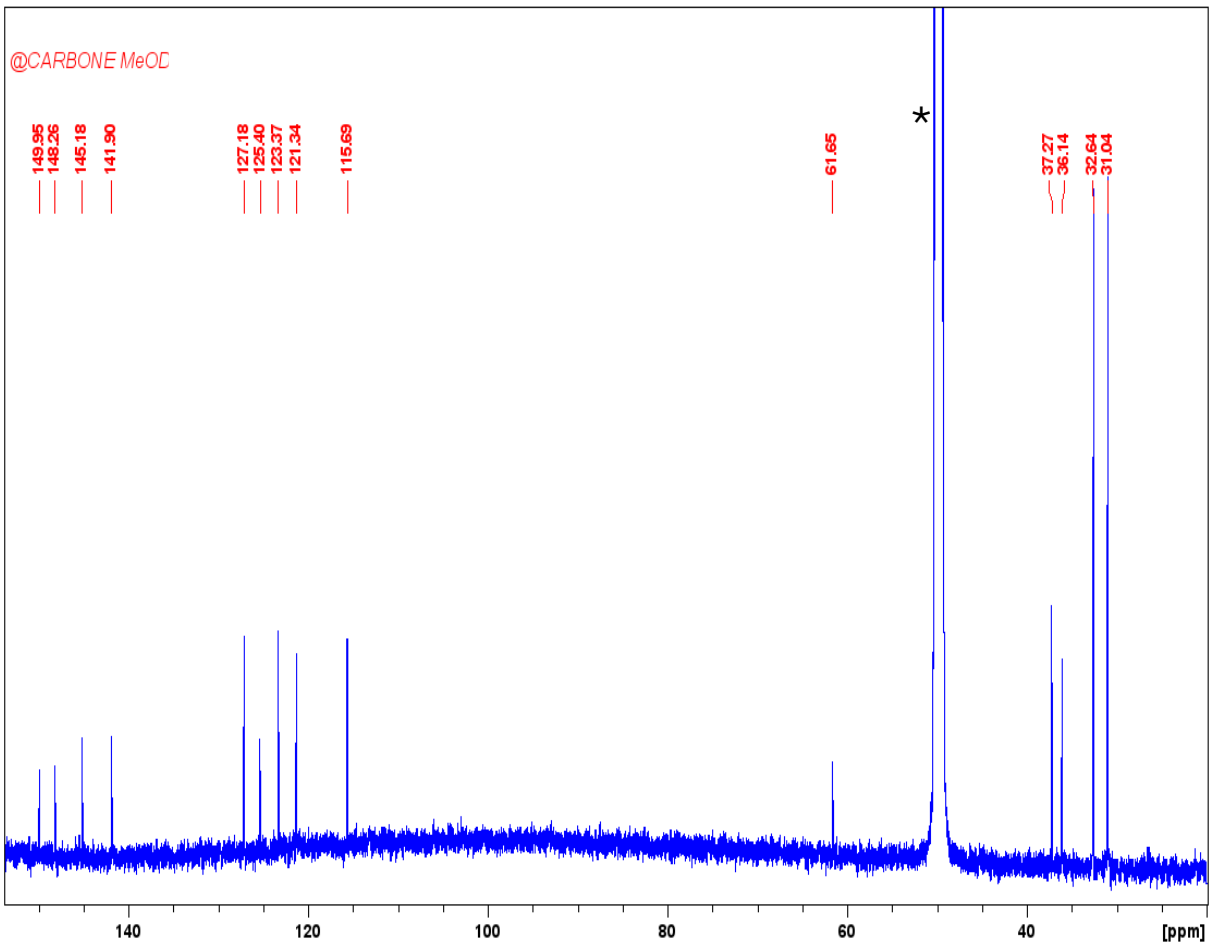

Figure S7. ^{13}C NMR spectrum of N-insertion product **[H$_2$L^{C2O2}(N)]Cl** in CD$_3$OD. Residual solvent from recrystallization marked with asterisks.

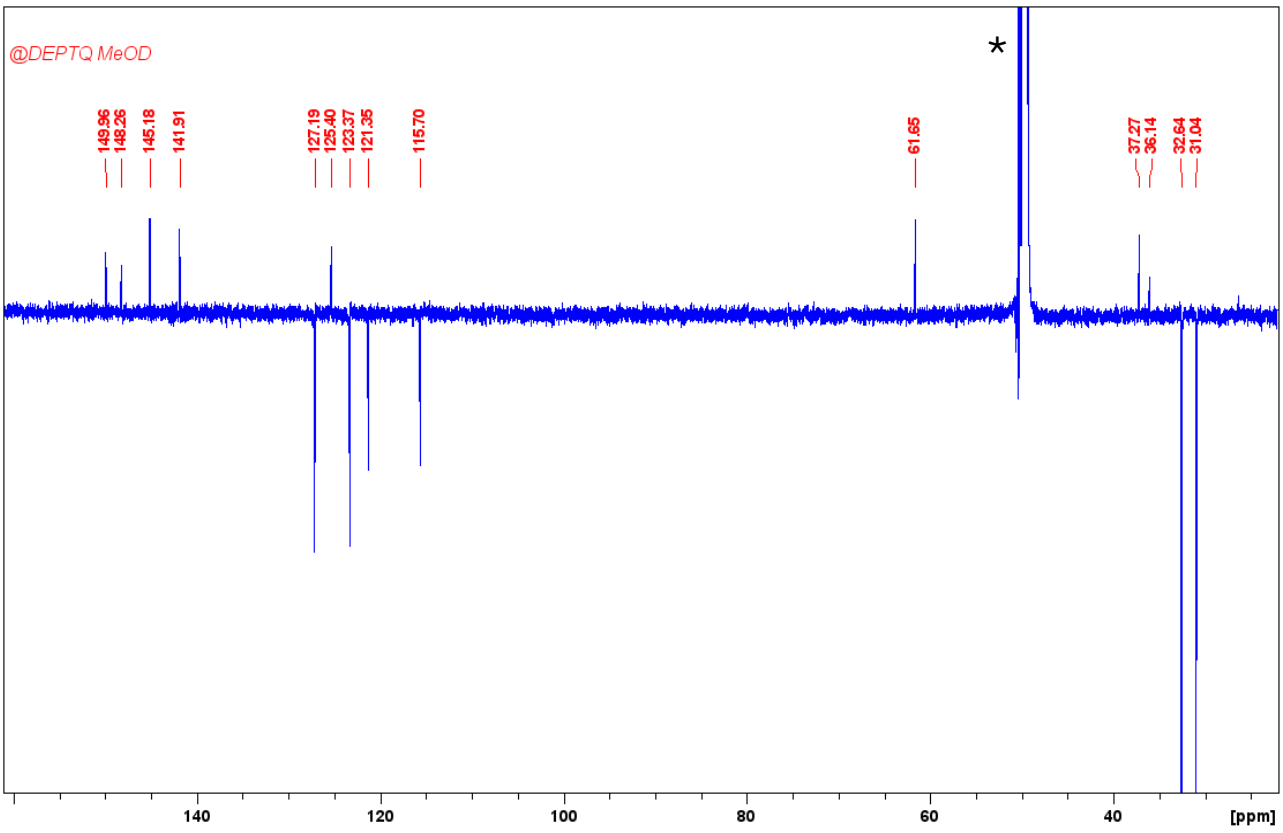

Figure S8. ^{13}C DEPT NMR spectrum of N-insertion product **[H$_2$L^{C2O2}(N)]Cl** in CD_3OD. Residual solvent from recrystallization marked with asterisks.

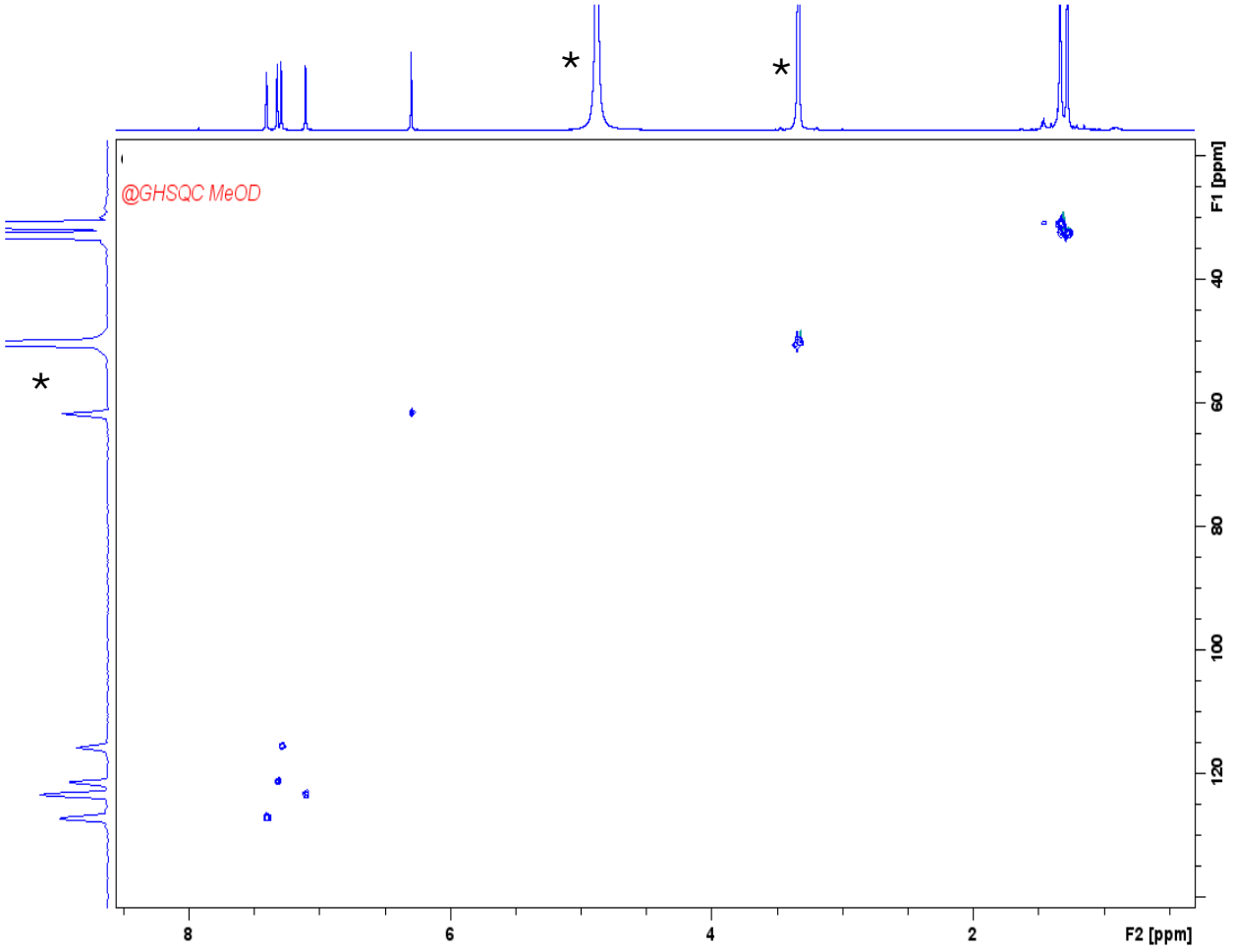

Figure S9. ^{1}H-^{13}C gHSQC NMR spectrum of N-insertion product **[H_2L^{C2O2}(N)]Cl** in CD_3OD. Residual solvent from recrystallization marked with asterisks.

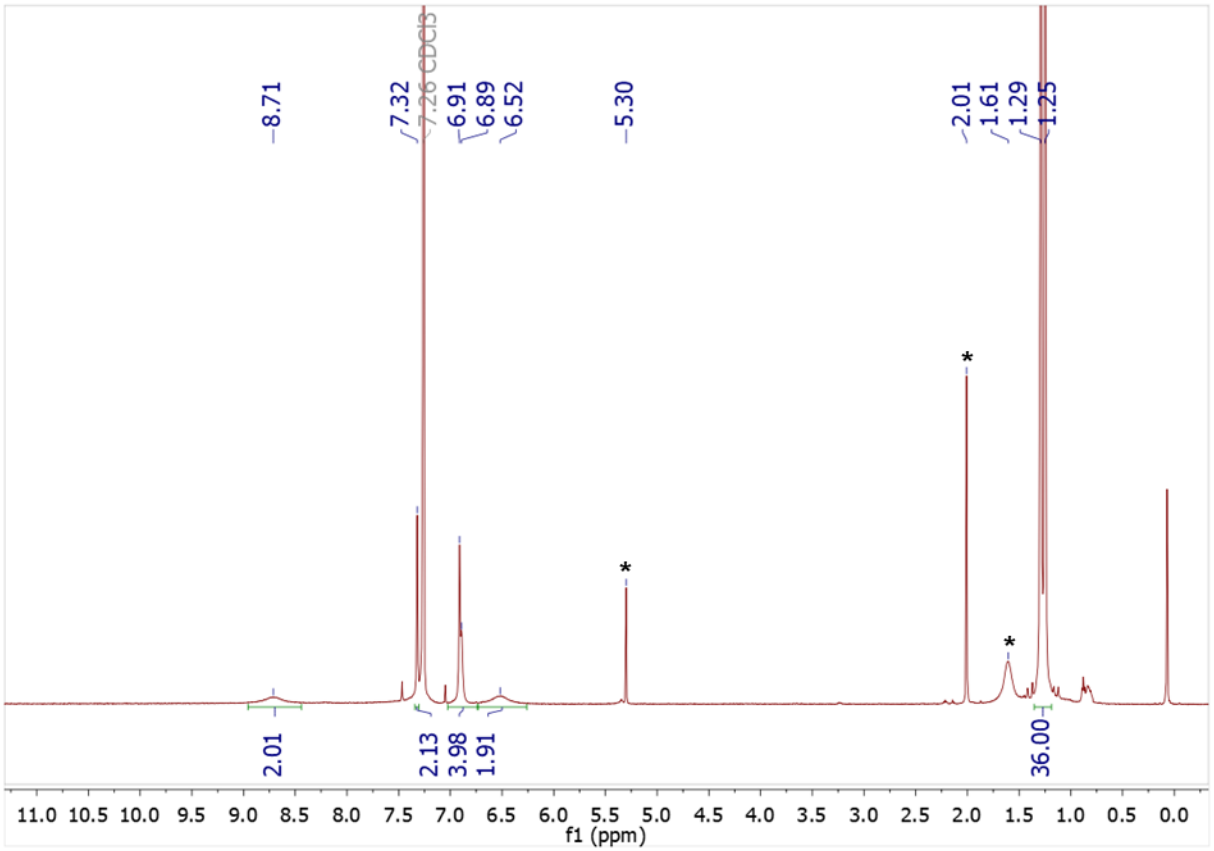

Figure S10. ^{1}H NMR spectrum of N-insertion product **[H_2L^{C2O2}(N)]Cl** in $CDCl_3$. Residual solvent from recrystallization marked with asterisks.

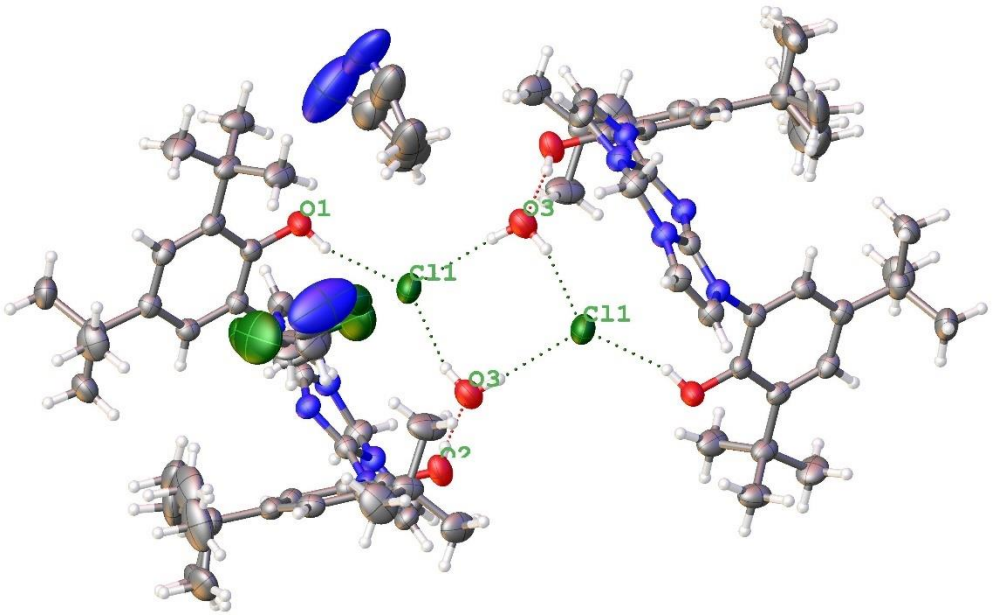

Figure S11. Hydrogen bond network in **[H_2L^{C2O2}(N)]Cl**.

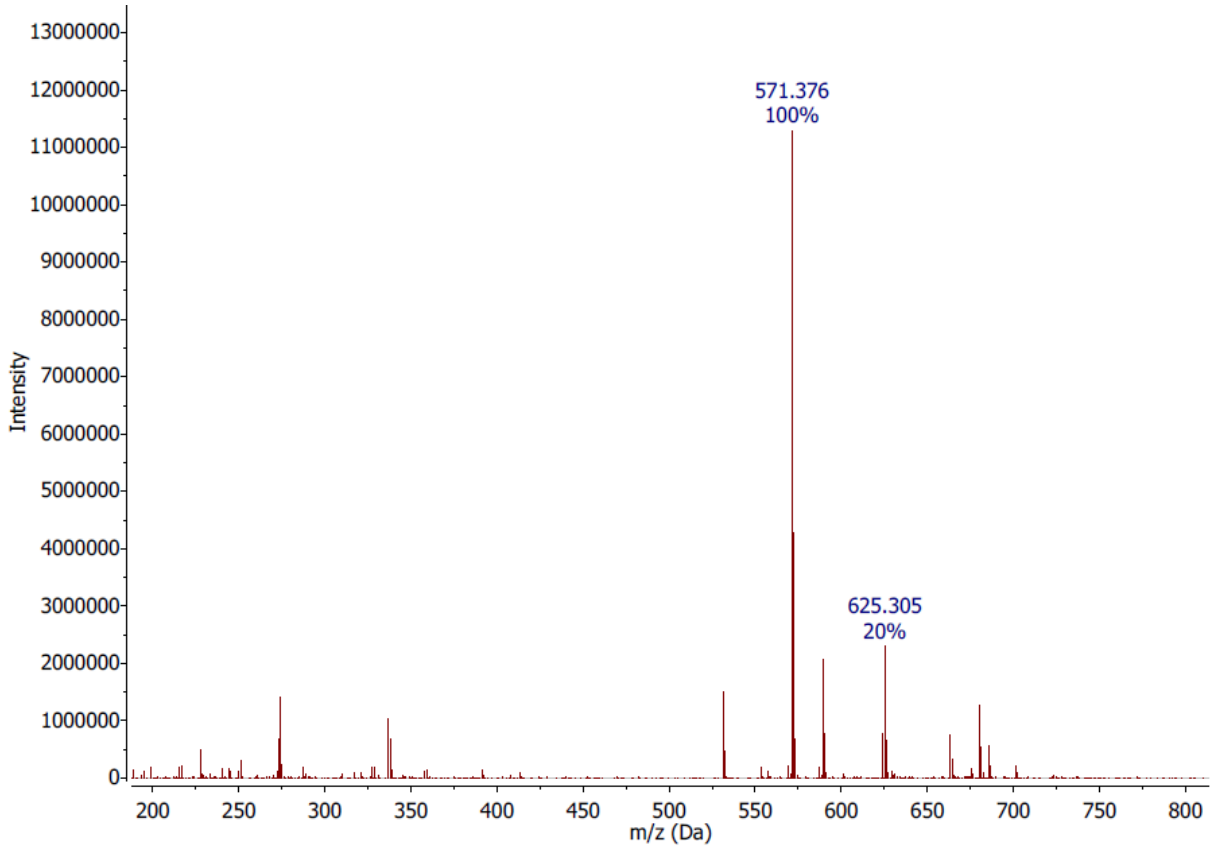

Figure S12. Positive mode ESI-MS analysis of the nitride exchange reaction between **Mnsalen(^{15}N)** and **MnL^{C2O2}(Br)** in CH_3CN.

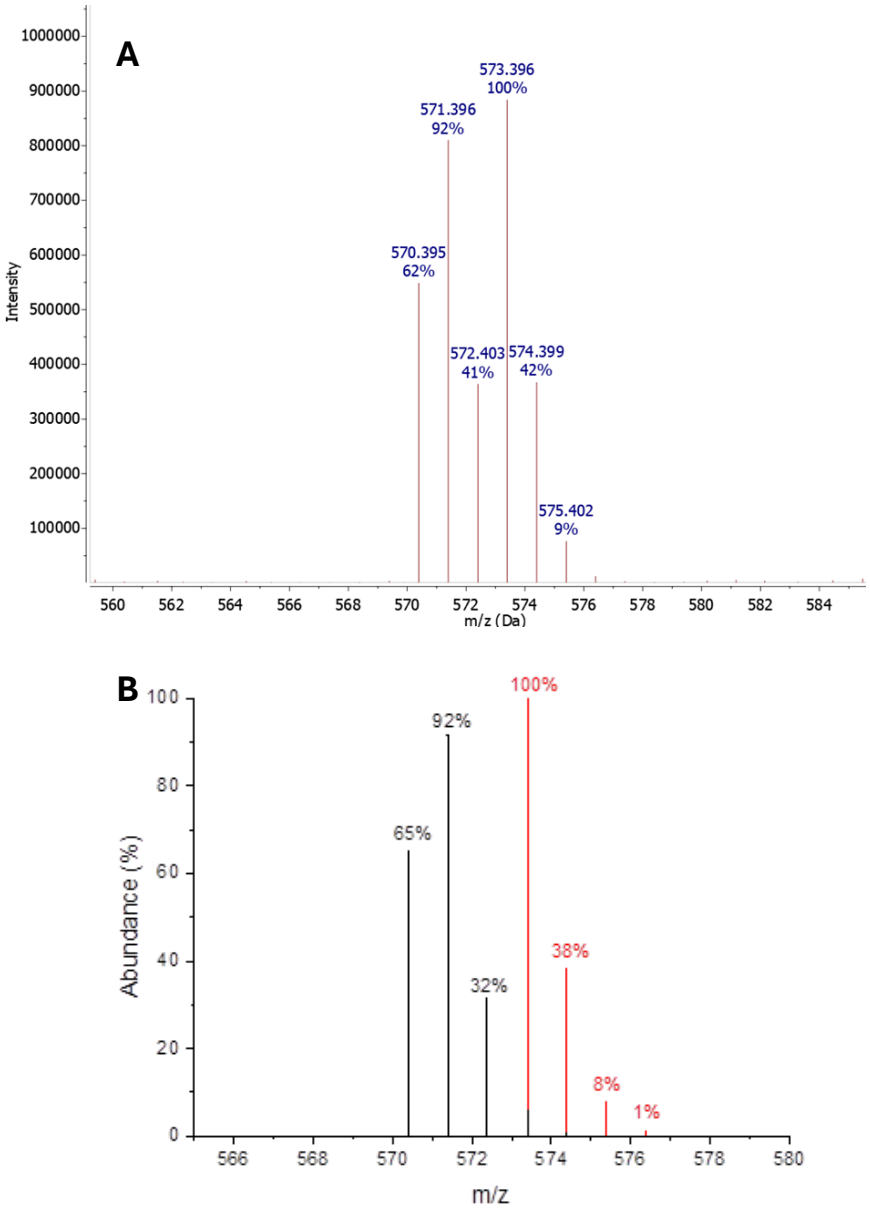

Figure S13. (A) Positive mode ESI-MS analysis of the photolysis of **MnL^{C2O2}($^{14/15}$N$_3$)** (λ_{ex} = 312 nm). (B) Predicted isotopic pattern for N-inserted ligand product (black) and O-inserted ligand product (red).

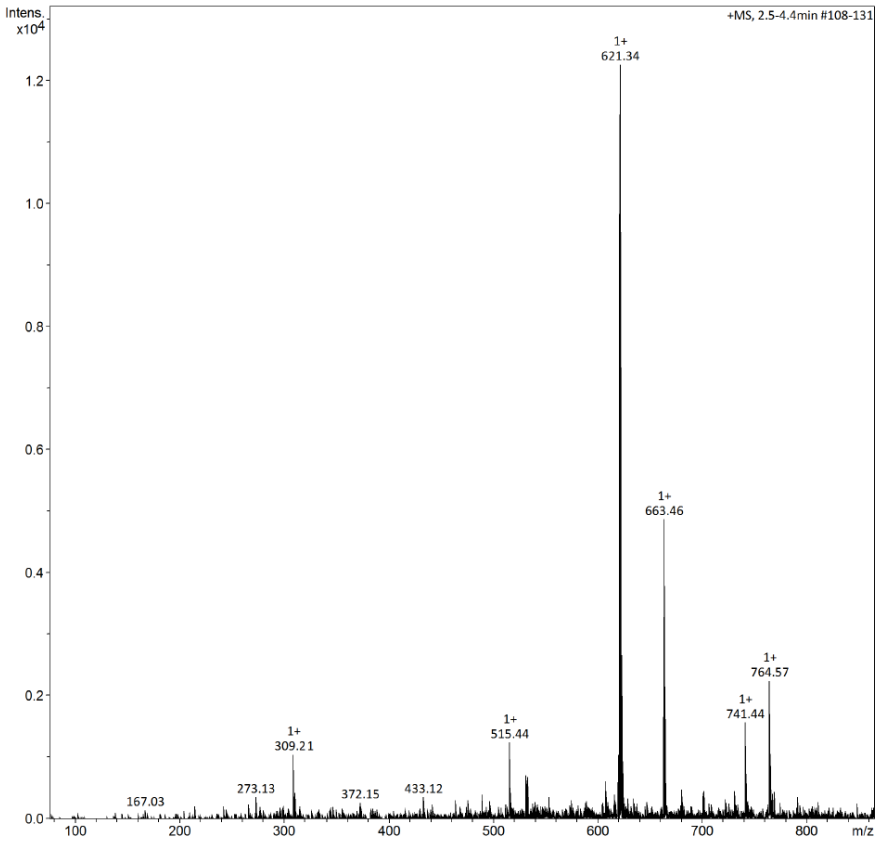

Figure S14. Positive mode ESI-MS analysis of **CrL^{C2O2}(N)**.

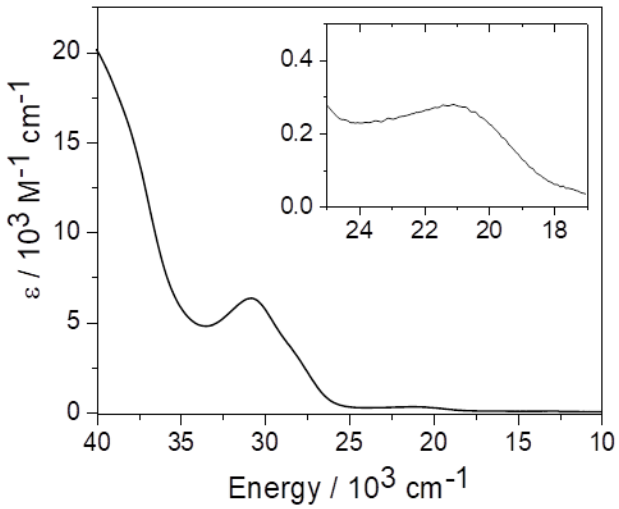

Figure S15. UV-vis-NIR spectra of a CH_2Cl_2 solution of **CrL^{C2O2}(N)**. T = 298 K. The observable $d \rightarrow d$ transition is highlighted in the inset.

Table S2. Crystal data and structure refinement for **CrL^{C2O2}(N).**

Compound	**CrL^{C2O2}(N)**
CCDC number	2359455
Formula	$C_{35}H_{46}CrN_5O_2$
F_w [g.mol^{-1}]	620.77
T [K]	296.15
Morphology	Prism
Color	Orange
Crystal size [mm]	0.14 x 0.33 x 0.45
Crystal system	monoclinic
Space group	-$P2_1/c$
a [Å]	15.7083(10)
b [Å]	12.5593(9)
c [Å]	16.5802(11)
α [°]	90
β [°]	96.354(2)
γ [°]	90
Unit-cell volume [Å^3]	3250.9(4)
Z	4
Dx [g.cm^{-3}]	1.268
μ [mm^{-1}]	0.391
F(000)	1324.0
Radiation	MoKα (λ = 0.71073)
Θ range for data collection/°	2.04 to 30.59
Index ranges	-22 ≤ h ≤ 22 -17 ≤ k ≤ 17 -23 ≤ l ≤ 23
Total reflections	93516
Unique reflections	9981
Used reflections	8454 (I>2σ(I))
Refined parameters	400
Rint.	0.0392
R1	0.0337
R(w)[a]	0.0962
Goodness of fit S	1.026
$\Delta\rho_{min}/\Delta\rho_{max}$ (e·Å^{-3})	-0.42/0.71

[a]Based on F^2 where $w = 1/[s^2(Fo^2)+(0.1P)^2]$ where $P=(Fo^2+2Fc^2)/3$ for **CrL^{C2O2}N**
$w = 1/[s^2(Fo^2)+(0.2000P)^2]$ where $P=(Fo^2+2Fc^2)/3$ for **$[3CrL^{C2O2}(\mu\text{-}N)_2]^+$**

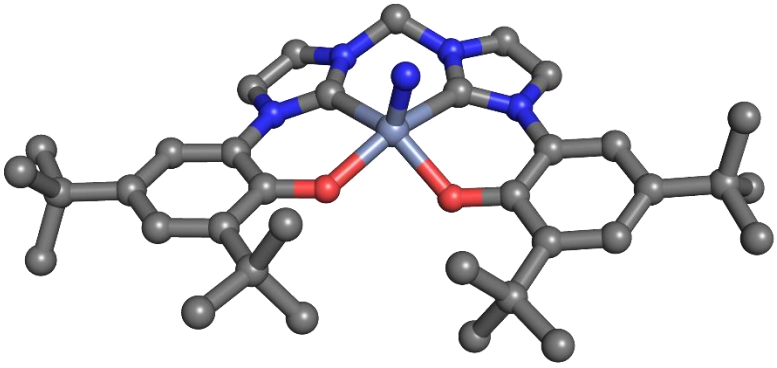

Figure S16. Predicted structure for the neutral **CrL^{C2O2}(N)** complex. See Experimental Section for calculation details.

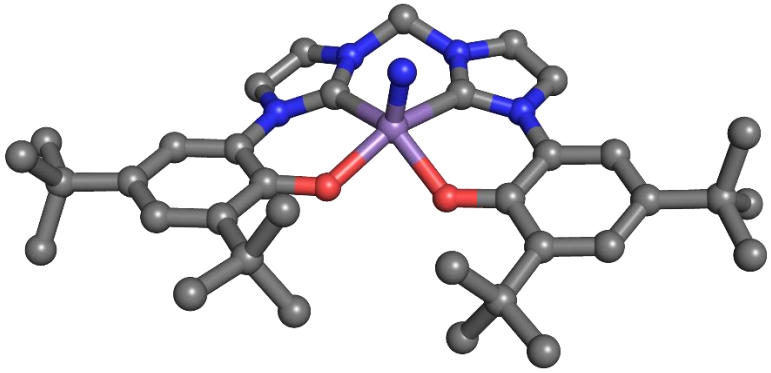

Figure S17. Predicted structure for the neutral **MnL^{C2O2}(N)** complex. See Experimental Section for calculation details.

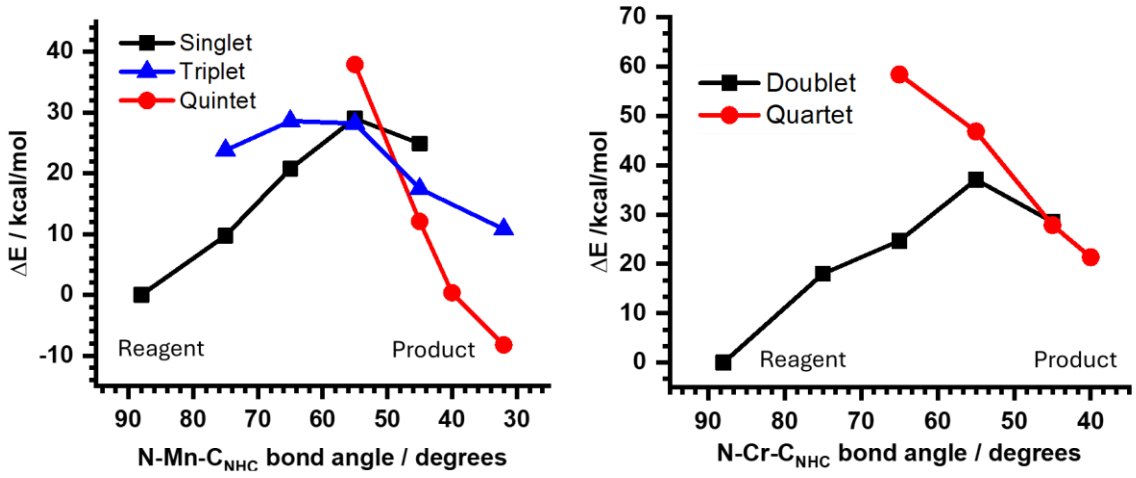

Figure S18. Potential energy surface (PES) for the nitride insertion reaction of **MnL^{C2O2}(N)** (Left) and **CrL^{C2O2}(N)** (Right). X-axis indicates change in Carbene-M-nitride bond angle from *ca.* 90° towards the transition state and finally inserted product.

Table S3. Relative spin state energetics of the ^{1}TS and ^{3}TS for the predicted nitride insertion reaction for **MnL^{C2O2}(N)**.

Theory Level	^{1}TS Relative Energy (kcal/mol)	^{3}TS Relative Energy (kcal/mol)
Opt: uB3LYP-GD3/6-31g* SP: uBP86-GD3/TZVP	0	-1.93
Opt/SP: wB97XD/TZVP	0	-6.89
Opt/SP: UMO6/TZVP	0	-14.33
Opt/SP: PBE-GD3/TZVP	0	-8.17

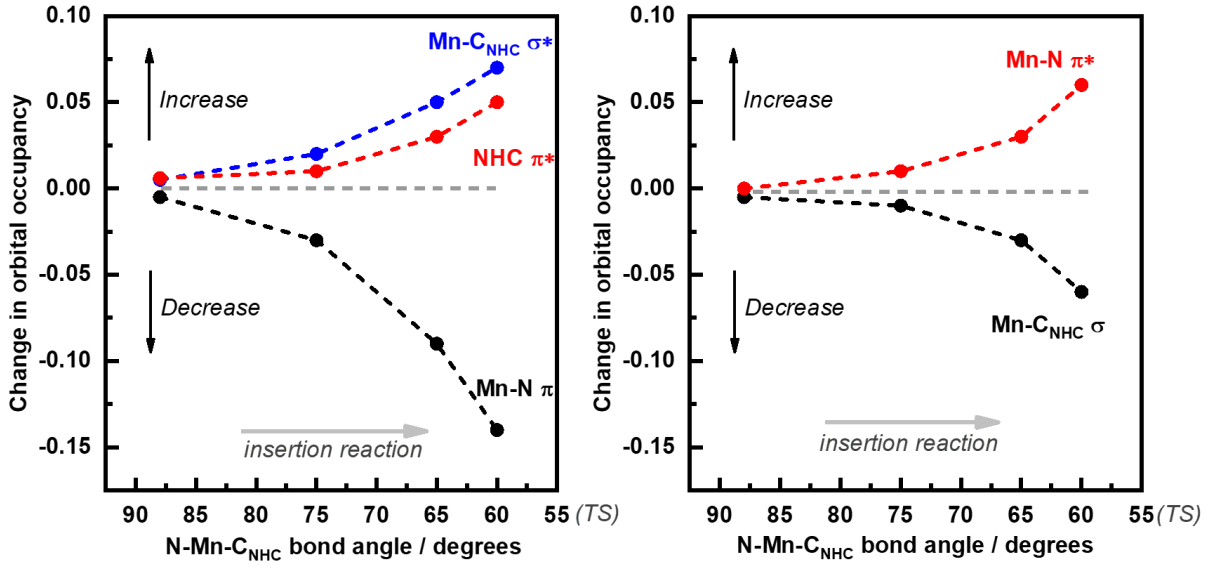

Figure S19. Predicted change in orbital occupancy for **MnL^{C2O2}(N)** as the N-Mn-C$_{NHC}$ bond angle is decreased from the equilibrium structure (*ca*. 90°) to the TS (*ca*. 60°) during the nitride insertion reaction. (Left) π Mn≡N donation, and (Right) σ Mn-NHC donation.

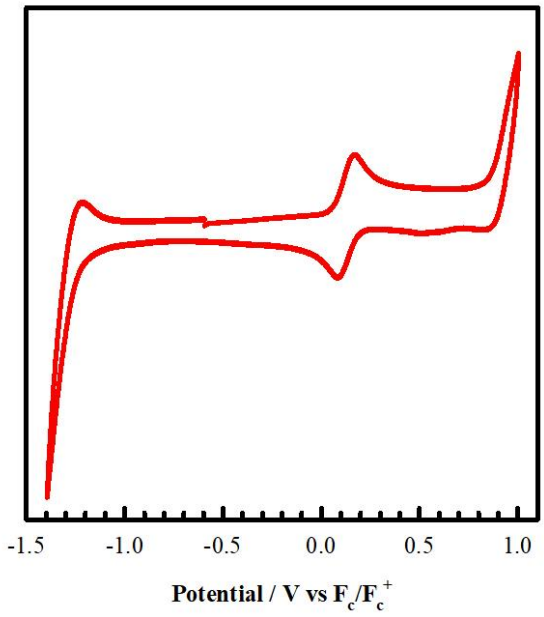

Figure S20. Cyclic voltammogram of **CrL^{C2O2}(N)** showing the full scan range. Conditions: 0.5 mM complex, CH_2Cl_2, 0.1 M TBAP, scan rate = 100 mV/s, 298 K.

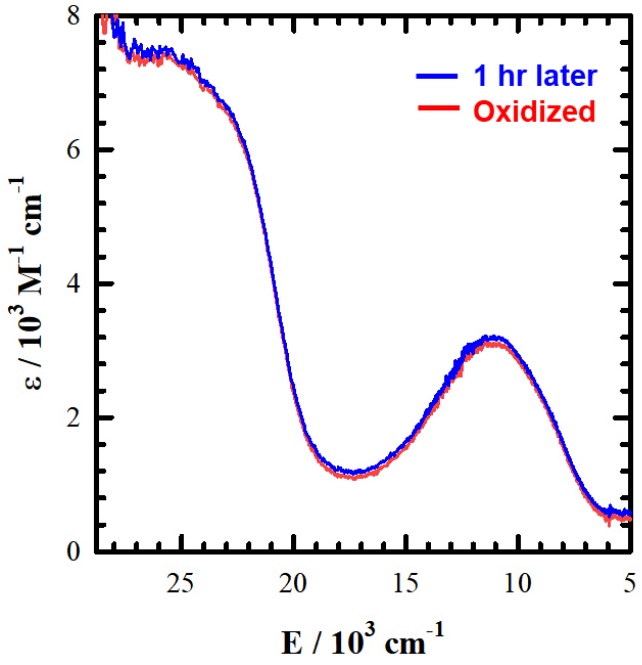

Figure S21. Stability of $[\mathbf{CrL^{C2O2}(N)}]^{+}$ over a one hour period. Conditions: 0.45 mM, CH_2Cl_2, 253 K.

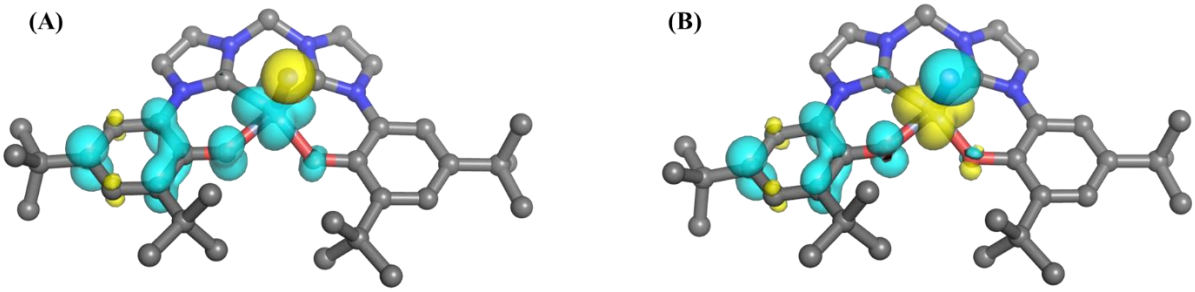

Figure S22. Spin density plots for (A) triplet $\mathbf{[CrL^{C2O2}(N)]^{+}}$ and (B) broken symmetry $\mathbf{[CrL^{C2O2}(N)]^{+}}$ electronic structures. See Experimental Section for calculation details.